Since January 2020 Elsevier has created a COVID-19 resource centre with free information in English and Mandarin on the novel coronavirus COVID-19. The COVID-19 resource centre is hosted on Elsevier Connect, the company's public news and information website.

Sustainable Cities and Society 74 (2021) 103226

Contents lists available at ScienceDirect

Sustainable Cities and Society

journal homepage: www.elsevier.com/locate/scs

Removal of SARS-CoV-2 using UV+Filter in built environment

Zhuangbo Feng [a], Shi-Jie Cao [a,b,*], Fariborz Haghighat [c]

[a] School of Architecture, Southeast University, 2 Sipailou, Nanjing, 210096, China
[b] Global Centre for Clean Air Research (GCARE), Department of Civil and Environmental Engineering, Faculty of Engineering and Physical Sciences, University of Surrey, Guildford, United Kingdom
[c] Department of Building, Civil and Environmental Engineering, Concordia University, Montreal, Canada

ARTICLE INFO

Keywords:
SARS-CoV-2
Air filter
UV
COVID-19 control
Airborne disease prevention
Energy saving

ABSTRACT

Air cleaning is an effective and reliable method in indoor airborne SARS-CoV-2 (Severe Acute Respiratory Syndrome Corona-Virus 2) control, with ability of aerosol removal or disinfection. However, traditional air cleaning systems (e.g. fibrous filter, electrostatic removal system) have some risks in operation process, including re-aerosolization and electric breakdown. To avoid these risks, the current study proposed an UV+Filter (ultraviolet and fibrous pleated filter) system to efficiently capture airborne SARS-CoV-2 aerosols and deactivate them in filter medium. It is challenging to quantitatively design UV+Filter due to complex characteristics of SARS-CoV-2 aerosols (e.g. aerodynamic size, biological susceptibility) and hybrid filtration/disinfection processes. This study numerically investigated the overall performances of different air cleaning devices (e.g. Fibrous-filter, UV+Filter, two-stage ESP (electrostatic precipitator) et al.) for control of SARS-CoV-2 aerosols and compared them in term of filtration efficiency, energy consumption and secondary pollution. The prediction of developed models was validated with the experimental data from literature. UV+Filter is the most reliable and safest, while its energy consumption is highest. The newly proposed design method of air cleaning systems could provide essential tools for airborne diseases control.

1. Introduction

The current outbreaks of corona-virus disease 2019 (COVID-19), induced by severe acute respiratory syndrome corona-virus 2 (SARS-CoV-2), have yet caused severe threats to global health and economy (Beria & Lunkar, 2020; Hosseini, Fouladi-Fard, & Aali, 2020; Rahman et al., 2020; Wang, 2021; WHO, 2020; Xu, Luo, Yu, & Cao, 2020). Reported transmission pathways of SARS-CoV-2 include: 1) direct inhalation of droplets produced by infected persons; 2) close contact with infected persons; 3) contact with polluted surfaces (Liu et al., 2020; Loey, Manogaran, Taha, & Khalifa, 2020). Moreover, aerosol transmission of pathogens has been proven as an important pathway based on the recent researches (Buonanno, Stabile, & Morawsk, 2020; Liu et al., 2020; Zhao, Liu, & Chen, 2020). Airborne precautions of SARS-CoV-2 have been adopted by public organizations and health authorizes (CDC, 2019; NCCEH, 2020; WHO, 2020).

For control of airborne transmission in indoor environment, ventilation and air purification are two effective ways (Bhattacharyya, Dey, Paul, & Biswas, 2020; Buonanno et al., 2020; Cao & Ren, 2018; Correia, Rodrigues, Gameiro, & Gonçalves, 2020; Ding, Yu, & Cao, 2020; Leng, Wang, & Liu, 2020; Yeo, Hosein, & Gregor-Davies, 2020; Yüksel, Arıcı, Krajčík, & Karabay, 2020). However, if ventilation and air purification systems are not properly designed or operated, they may contribute to the transmission/spreading of airborne diseases and heat/moisture in indoor environment (Correia et al., 2020; Luo, Huang, Feng, Li, & Gu, 2021). This could be the case when the filtration system cannot efficiently remove the aerosols before being mixed with supply air, resulting in accelerating the spread of virus in the indoor environment. Besides, aerosols, like SARS-CoV-2, can deposit on duct surfaces, causing resuspension risk of virus. If exhaust ducts are not equipped with air purification devices, SARS-CoV-2 aerosols can be released into atmospheric environment, which may cause a potential threat to the surrounding environment (Correia et al., 2020). Therefore, air purification system should be effectively utilized in ventilation system to effectively control spread of SARS-CoV-2 aerosols in built environment (Correia et al., 2020; Zhao et al., 2020).

Air cleaning technologies have been proven to be effective methods in indoor air quality control (Charvet, Pacault, Bourrous, & Thomas, 2018; Malayeri, Haghighat, & Lee, 2021, 2020; Shyegan, Haghighat, & Lee, 2020; Wang, Haghighat, & Mortazavi, 2009; Zhong, Lee,

* Corresponding author.
E-mail address: shijie_cao@seu.edu.cn (S.-J. Cao).

https://doi.org/10.1016/j.scs.2021.103226
Received 11 January 2021; Received in revised form 31 July 2021; Accepted 31 July 2021
Available online 3 August 2021

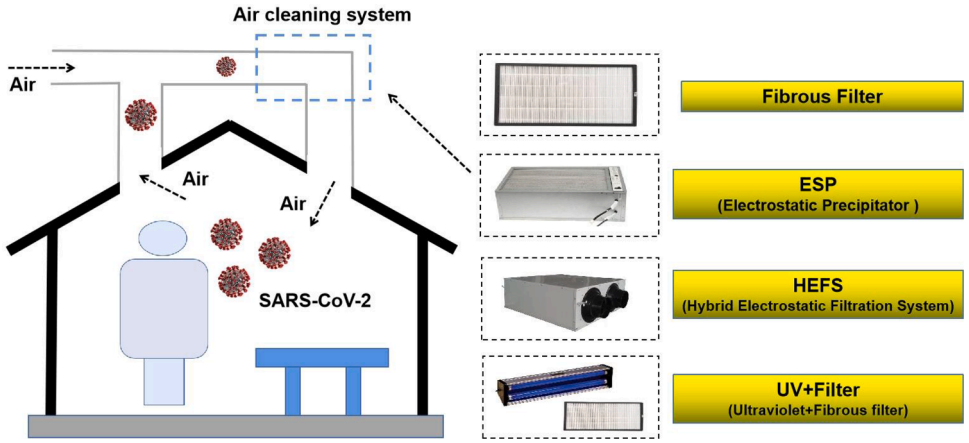

Fig. 1. The role of air cleaning technologies in indoor ventilation system for SRAS-CoV-2 control and widely used types of air cleaning devices.

Haghighat, & Bahloul, 2016). Recently, extensive research has been conducted to optimize ventilation designs in reference to SARS-CoV-2 aerosols control (Leng et al., 2020; Vuorinen et al., 2020; Wang, Huang, Feng, Cao, & Haghighat, 2021). However, available literatures are insufficient to focus on the purification/filtration of SARS-CoV-2. Fibrous filter, electrostatic removal device and ultraviolet germicidal irradiation (UV) are potential devices for SARS-CoV-2 removal/disinfection. The main control mechanism of fibrous filter and UV is physical filtration and biological disinfection, respectively (Abdolghader, Haghighat, & Bahloul, 2018; Charvet et al., 2018; Saleh et al., 2014; Velali et al., 2020; Yang, Zhang, Nunayon, Chan, & Lai, 2018). Electrostatic removal devices (e.g. ESP) are able to simultaneously remove the particle as well as deactivate it by ions (Feng & Cao, 2019; Feng, Cao, Wang, Kumar, & Haghighat, 2021).

The widely used air cleaners (fibrous filter, UV and electrostatic removal devices) have some disadvantages, from the perspectives of SARS-CoV-2 aerosol control. Previous studies reported that fibrous filter (e.g. HEPA, high efficiency particulate air filter) could have ultra-high filtration efficiency for SARS-CoV-2 aerosols (Charvet et al., 2018). The disadvantages of fibrous filter include high pressure drop, energy consumption and replacement cost (Feng, Long, & Yu, 2016). Besides, bacterium can propagate in fibrous filter with loaded cake layer, therefore inducing health risk/secondary contamination during maintenance and replacement due to re-aerosolization (Nakpan, Yermakov, Indugula, Reponen, & Grinshpun, 2019; Bahrami , Haghighat, & Bahloul, 2021). UV has been proven to be effective for disinfection of many airborne biological species (Yang et al., 2018; Yang, Zhang, Chan, & Lai, 2019). Many literatures have concluded that UV can effectively inactivate SARS-CoV-2 aerosols deposited on solid surfaces and porous mediums (Fischer et al., 2020; Heilingloh et al., 2020; Sarkis-Onofre et al., 2020). However, research focusing on UV disinfection of airborne SARS-CoV-2 aerosols and its UV susceptibility is hardly available: without UV susceptibility coefficient, it is difficult to accurately design UV device towards SARS-CoV-2 control. Typical electrostatic removal devices include electrostatic precipitator (ESP) and hybrid electrostatic filtration system (HEFS) combining ESP and fibrous filter in series (Feng et al., 2016, 2018b). Earlier studies proved that the well-designed ESP/HEFS could have very high physical filtration efficiency for airborne aerosols (Feng, et al., 2018b), and ions generated by corona discharge could effectively deactivate biological species (Zhou, Yang, Lai, & Huang, 2016). However, the ability of electrostatic devices to remove/inactivate SARS-CoV-2 aerosols has not yet been tested. In terms of control of SARS-CoV-2 aerosols with a high toxicity, the re-aerosolization risk of fibrous filter and electric-breakdown risk of ESP may significantly increase exposure and infection, causing great threat to human safety. Therefore, it is very necessary to develop a safe, reliable and high-efficient air cleaning system towards the control of SARS-CoV-2 aerosols with a high toxicity.

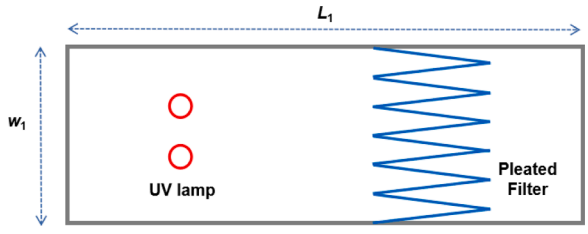

Fig. 2. Configuration of UV+Filter system with geometric parameters.

To avoid the risks/limitations of widely used air cleaning types, the current study proposed an UV+Filter (ultraviolet and fibrous pleated filter) system to efficiently capture airborne SARS-CoV-2 aerosols and deactivate them by UV lights. It is quite challenging to quantitatively design UV+Filter due to the complex characteristics of SARS-CoV-2 aerosols (e.g. aerodynamic size, biological susceptibility) and multiple-physical phenomena (e.g. porous medium flow, UV irradiance). To accurately simulate its performance, it is urgent to develop a quantitative methodology to analyze multiple-physics fields in UV+Filter and obtain filtration/disinfection efficiency. Beside, there is a need to investigate the performance of UV+Filter and compare its overall filtration performance with various air purification types in term of filtration/disinfection efficiency, energy conservation, and exposure risk.

The current study aims to propose an UV+Filter system to high-efficiently remove and disinfect airborne SARS-CoV-2 aerosols. A multiple-physics model (e.g. porous medium flow, UV irradiance, aerosol filtration/disinfection) was utilized to simulate and design UV+Filter system. First, the main characteristics of SARS-CoV-2 aerosols were summarized, including aerodynamic characteristics and susceptibility to UV lights. Next, a multiple-physics model of UV+Filter was developed which included porous medium flow, aerosol filtration/disinfection, and UV dose applied to pleated filter. Then, the numerical model was adopted to properly design the UV+Filter system in order to obtain satisfactory filtration/disinfection performances. Finally, the SARS-CoV-2 aerosol removal/disinfection performance of ESP/HEFS were investigated through numerical simulation while overall filtration performances of different properly designed air cleaning types (e.g. selection of fibrous medium, arrangement of discharge wires in ESP/HEFS) were analyzed/evaluated (as shown in Fig. 1), including energy consumption, secondary pollution generation and operation risk level.

2. Methodology

The numerical models for UV+Filter system are described and the

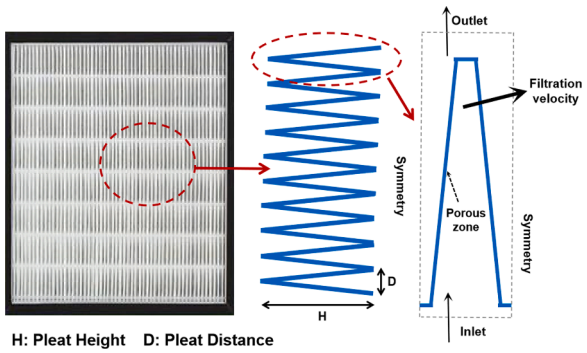

Fig. 3. Geometry of fibrous pleated filter and definitions of pleat parameters.

models of two electrostatic cleaning systems (ESP and HEFS) are then briefly introduced.

2.1. UV+Filter system

The UV+Filter system consists of a UV generator (lamps) and fibrous pleated filter in series. The UV light leaving the lamp reaches the pleated filter surface and deactivates SARS-CoV-2 aerosols in the filter medium. Besides, the UV light can also inactivates biological aerosols in air. Numerical models of pleated filter and UV irradiance field were individually described as follows: Fig. 2 shows the geometry of UV+Filter system, in which UV (ultraviolet germicidal irradiation) lamps and fibrous pleated filter were installed in series. Two cylindrical lamps were placed in duct zone. The diameter of each cylindrical lamp was 10 mm. The width of simulation domain (w_1) was 250 mm.

The geometry of fibrous pleated filter is shown in Fig. 3. In order to increase filtration efficiency, the pleat structure was adopted to effectively enlarge filter surface area and decrease filtration velocity. The aforementioned figure shows that filtration velocity (m/s) is defined as the quotient of airflow rate (m^3/s) divided by surface area (m^2) of fibrous pleated filter. Due to its periodicity, only one pleat was adopted to show its structure. Different boundary types were described in Fig. 3, including "Inlet", "Outlet", "Symmetry" and "Porous Zone"; two structural parameters, pleat height (H) and pleat distance (D), were also defined.

Numerical modeling of fibrous filters consists of two steps: air flow and particle filtration modeling. The filter media was modeled as a porous zone and its permeability constant for a porous medium was calculated by the Carman–Kozeny expression Feng, Pan, Wang, & Long, 2018a). In the porous zone, source terms (S_i) were added to the momentum equation, as described in Eq. (1). For the fibrous filter medium, the viscous resistance is dominant and inertial resistance could be ignored. The flow field through the porous filter medium was simulated by solving Navier-Stokes equations with viscous resistance in the porous zone. This study used SIMPLE algorithm (rather than COUPLE algorithm) to couple air pressure and velocity because of the relatively simple pleat structure. Once air velocity distributions were obtained, particle trajectory and filtration effect were simulated by the Lagrangian method and filtration efficiency model (as described by Eqs. (2) and ((3)). Detailed information about fibrous filter modeling could be found in (Feng et al., 2018a).

$$S_i = -\left(\frac{\mu}{\beta}u_i + C_2\frac{\rho}{2}|u_i|u_i\right) \tag{1}$$

$$\frac{d\overrightarrow{u_P}}{dt} = F_D\left(\overrightarrow{u} - \overrightarrow{u_p}\right) + \frac{\overrightarrow{g}\left(\rho_p - \rho\right)}{\rho_p} + \overrightarrow{F_a} \tag{2}$$

$$E_T = 1 - \exp\left[-(4\alpha \times eff \times Z_T)\,/\,\left((1-\beta)d_f\pi\right)\right] \tag{3}$$

where u_p is the particle velocity vector (m/s), u is the air velocity vector

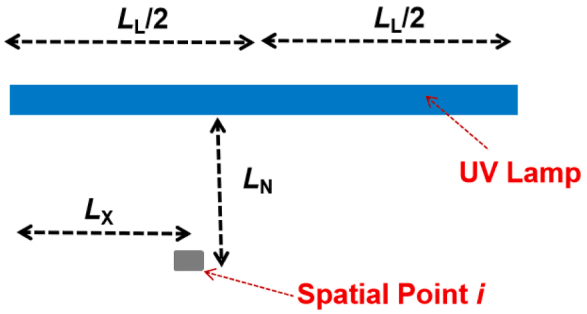

Fig. 4. Schematic diagram of view factor calculation for in-duct UV devices.

(m/s), t is the time (s), the i represents coordinates (e.g. x, y, z), β is the permeability of porous medium (m^{-2}), C_2 is the inertial resistance factor of porous medium (m^{-1}), g is the gravitational acceleration (m^2/s), ρ is the air density (kg/m^3), ρ_p is the particle density (kg/m^3), F_D is the inverse of the relaxation time (m^{-1}), F_a stands for the additional forces (N, such as electrostatic force acting on charged particles), E_T is the removal ratio for a certain particle trajectory in one time step, α is the solid ratio of filter medium, eff is the overall single fiber efficiency (including effects of diffusion, interception, impaction and electrostatics), d_f is the fiber size, and Z_T is the particle trajectory length in one time step. For fibrous filter simulation, C_2 is zero due to the fact that inertial resistance could be ignored. For numerical modeling of fibrous filter, the air temperature and humidity could influence air viscosity, further influence F_D (Eq. (2) in the current study) and particle motion/filtration in porous filter medium (Zhao, Chen, Yang, & Lai, 2010). In the current study, room air parameters (25 °C, 60%) were adopted. In our future study, the effects of air temperature/humidity on air filtration will be investigated by using experiments and numerical simulation.

The key design parameters of fibrous pleated filter are the mean fiber diameter (d_f, μm), the mean packing density (α), and the filter thickness (Z, μm). The index of MERV (Minimum Efficiency Reporting Value) was adopted to classify different types of fibrous air filter (ASHRAE, 2017). In this study, five filter types were tested: Filter A (d_f: 1.6 μm; α: 0.076; Z: 800 μm; MERV 19), Filter B (d_f: 5.1 μm; α: 0.074; Z: 800 μm; MERV 10), Filter C (d_f: 2.2 μm; α: 0.050; Z: 800 μm; MERV 14), Filter D (d_f: 26.8 μm; α: 0.241; Z: 800 μm; MERV 6), Filter E (d_f: 16.9 μm; α: 0.217; Z: 800 μm; MERV 8). For all of the five types, pleat height and pleat distance were respectively set as 100 mm and 10 mm. The average filtration velocity was close to 2.5 cm/s, which is in the range recommended by engineering standards (GB/T 13554–2020). Filter A was a high-efficient type, while Filter B/C and Filter D/E were medium-efficient and coarse filter types, respectively. Numerical models were adopted to study the performance of the five filter types from the perspective of SARS-CoV-2 aerosols control. The best type was selected in reference to evaluations of different air cleaning devices.

In order to simulate disinfection efficiency of UV+Filter system with cylindrical UV lamp, UV irradiance field should be solved first, based on Eq. (4). The view factor $V_{i\text{-}L}$ is function of L, L_N and L_X, as described in Fig. 4. Detailed formula expression of Eq. (4) could be found in (Yang et al., 2019). The influences of UV irradiance field on air flow field were ignored and air momentum equations were directly solved by using CFD (Computational Fluid Dynamics). If fibrous filter was coated with photo-catalytic catalysts (deposited on fiber surface), UV light intensity may begin to attenuate across filter thickness (photon absorption) (Malayeri et al., 2021). Based on previous researches (Malayeri et al., 2021), UV absorption in fibrous pleated filter (without catalyst) could be negligible. We also utilized experimental method (Yang et al., 2019) to investigate the influences of fibrous filter (Filter A, without catalyst) on UV light intensity in duct system, and the UV absorption in Filter A was negligible. Overall, absorption of UV light in pleated filter without catalyst were assumed negligible in the current study

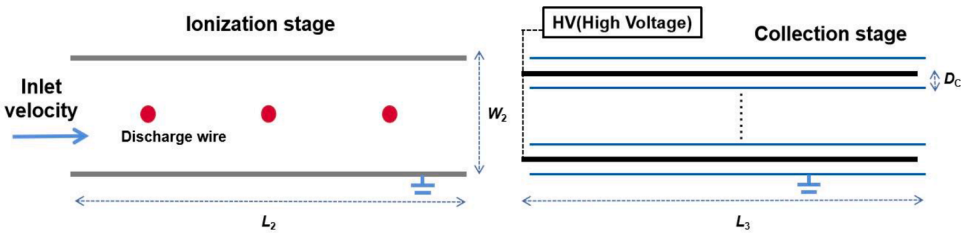

Fig. 5. The geometry of two-stage ESP and definitions of geometric parameters.

$$I_i = \frac{fP}{A_L} V_{i-L}(L_N, L_X, L/2) \tag{4}$$

In Eq. (4), I_i is the spatial irradiance for point i (W/m^2), f is the efficiency of cylindrical lamp power to be converted into the UV output power, P is the cylindrical lamp power (W), A_L is surface area of the cylindrical UV lamp (m^2), L_L is the length of UV lamp (m), $V_{i\text{-}L}$ is the view factor which represents the fraction of radiative energy leaving from viewpoint i and reaching the UV lamp.

Once UV irradiation field and turbulent airflow field were obtained, Eq. (5) was used in order to simulate disinfection efficiency of UV+Filter system. Disinfection efficiency could be determined based on biological particle concentration of inlet/outlet.

$$\frac{\partial C_i}{\partial t} + \nabla\cdot[(\vec{u} + v_s)C_i] = \nabla\cdot\left[(D + \varepsilon_p)\nabla C_i\right] - AI_R C_i \tag{5}$$

where C_i is the activated biological particle concentration (N/m^3), v_{si} is the particle settling velocity (m/s), u is the air velocity (m/s), t is the physical time (s), D is the Brownian diffusion coefficient (m^2/s), ε_p is the particle eddy diffusivity (m^2/s), I_R is the irradiance intensity (W/m^2), A is the susceptibility (disinfection coefficient) due to irradiance intensity (m^2/J).

2.2. Electrostatic removal systems

In the current study, two-stage ESP and HEFS were investigated towards the control of airborne SARS-CoV-2 aerosols. Traditional one-stage ESP, only including ionization stage, was not considered in the current study due to its high ozone generation Chen, Gonze, Ondarts, Outin, & Gonthier, 2020). The geometry of two-stage ESP is shown in Fig. 5. The ionization stage and collection stage were adopted to charge and capture incoming particles/aerosols, respectively. For the ionization stage, the Poisson equation and current continuity equation were simultaneously solved to obtain distributions of electric potential and space charge density, as described by Eqs. (6) and ((7). For the collection stage, Eq. (6) without space charge density (so-called Laplacian equation) was used to simulate electrostatic field intensity. The Lagrangian model (Eq. (2)), and particle charging model (Eq. (8)) were simultaneously utilized to simulate particle motion and charging in two-stage ESP and HEFS.

$$\nabla^2 V = -\frac{q}{\varepsilon_0} \tag{6}$$

$$\nabla\cdot\left(k_i \vec{E} q\right) = 0 \tag{7}$$

$$q_P = \frac{3\pi K_p \varepsilon_0 E d_p^2}{K_p + 2}\left(\frac{t}{t+\tau}\right) + \frac{2\pi\varepsilon_0 d_p kT}{e} Ln\left(1 + \frac{t}{\tau_c}\right) \tag{8}$$

where $\vec{E}$ is the electric field intensity vector (V/m), ε_0 is the air permittivity (F/m), where q_P is the particle charge amount (C), K_p is the particle dielectric constant, d_p is the particle diameter (m), t is the physical time (s), τ and τ_c are time constants, k is Boltzmann's constant (1.38E-23 J/K), e is the charge on an electron (1.6E-19 C), and T is temperature (K).

In Fig. 5, several critical geometrical parameters were defined:

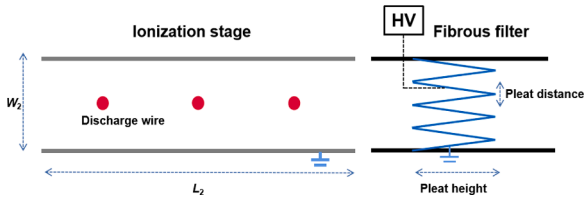

Fig. 6. The geometry of HEFS and definitions of geometric parameters.

Table 1
Summary of design information of various air cleaning devices.
(d_f: mean fiber diameter; α: mean packing density; Z: thickness of filter medium).

	UV device	Filter medium	Filter geometry
UV+Filter	Cylindrical UV lamp diameter (10 mm), Irradiance intensity (I_R) near the lamp surface (~ 340 W/m^2)	Filter A (d_f: 1.6 μm; α: 0.076), Filter B (d_f: 5.1 μm; α: 0.074), Filter C (d_f: 2.2 μm; α: 0.050), Filter D (d_f: 26.8 μm; α: 0.241), Filter E (d_f: 16.9 μm; α: 0.217). Filter A-E (Z: 800 μm)	Pleat distance (10 mm), Pleat height (100 mm)
	Ionization stage	**Collection stage**	
Two-stage ESP	Width of ionization stage (0.067 m), Length of ionization stage (0.3 m), Applied voltage in ionization stage (6.5–8.5 kV), Three discharge wires (radii: 0.0001 m)	Width of collection stage (0.067 m), Length of collection stage (1.0 m), Distance between two collection plates (0.007 m), Applied voltage between two collection plates (3 kV)	
	Ionization stage	**Filter medium**	**Filter geometry**
HEFS	Width of ionization stage (0.067 m), Length of ionization stage (0.3 m), Applied voltage in ionization stage (6.5–8.5 kV), Three discharge wires (radii: 0.0001 m)	Filter (d_f: 10 μm; α: 0.1; Z: 2 mm), The value of electrostatic intensity across filter medium thickness (1.2E+06 V/m)	Pleat distance (22.3 mm), Pleat height (100 mm)

length of ionization stage (L_2, 0.3 m), length of collection stage (L_3, 1.0 m), width of ionization stage (w_2, 0.067 m), and distance between two collection plates (D_C, 0.007 m). Three discharge wires with radii of 0.0001 m were uniformly distributed along the length direction. This study also investigated the performance of two-stage ESP with single discharge wire (installed in the central point) in the ionization stage. The applied voltage (V_i) in the ionization stage was 6.5–8.5 kV (positive voltage). The voltage (V_c) between two collection plates was 3 kV. The inlet air velocity of ESP was 1 m/s, as shown in Fig. 5. The configuration shown in Fig. 5 was a system unit of two-stage ESP. In practical conditions, more channels are needed and many units should be added together in order to meet practical requirements.

The geometry of hybrid electrostatic filtration system (HEFS), consisting of ionization stage and pleated filter, is shown by Fig. 6. The ionization stage of HEFS is the same as that of two-stage ESP. An

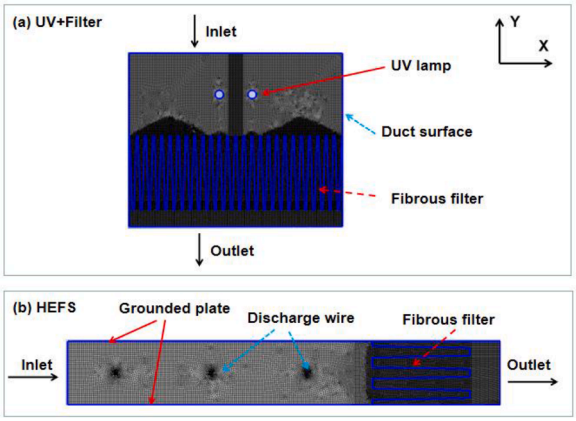

Fig. 7. Boundary conditions and mesh distributions of (a) UV+Filter and (b) HEFS.

electrostatic field was added across the thickness of fibrous filter medium. For the ionization stage, numerical models of ionized electric field and particle charging/motion were the same as the two-stage ESP. The Lagrangian model with electrostatic-enhanced single fiber efficiency model were adopted to simulate charged particle removal in the fibrous filter medium (Feng et al., 2018b).

In HEFS, the design parameters of fibrous filters found in literature were used: fiber diameter of 10 μm, solid packing density of 0.1, filter thickness of 2 mm (Feng et al., 2016). For the filter medium in HEFS, its level was MERV-9 (ASHRAE, 2017). Pleat height and pleat distance was 100 mm and 22.3 mm, respectively. The average filtration velocity was close to 0.1 m/s, which was higher than that of UV+Filter system (2.5 cm/s, 0.025 m/s). In UV+Filter and HEFS, high-efficient and medium-efficient filters were used respectively. Therefore, the values of filtration velocities were different due to the two different filtration grades. In HEFS, the electrostatic intensity across filter medium thickness was 1.2E+06 (V/m).

Table 1 summarizes the detailed design information of various air cleaning devices in the current study, including UV+Filter, two-stage ESP and HEFS systems.

2.3. Numerical methodology

For the UV+Filter system, three dimensional geometry and meshing strategy were utilized (Yang et al., 2018). The two-staged ESP and HEFS had two dimensional characteristics, and previous study proved that the two dimensional meshing strategy could provide satisfied simulation results (Feng et al., 2018b). Therefore, two dimensional geometry and meshing strategy were adopted in the current study to investigate the performance of ESP and HEFS.

For UV+Filter system, the ANSYS-FLUENT platform was utilized to simulate UV field, turbulent air flow and biological particle disinfection/filtration. User-Defined Functions (UDF) were developed to simulate the distributions of UV irradiance intensity. Fig. 7 shows the mesh distributions in XY plane (as described in Figs. 3, 5, and 6 in this paper). The mesh distributions of XY plane remain the same pattern along Z direction. The hexahedral meshes were used, and total element number was 4.2 million. Local meshing refinement was used in the pleated filter medium zone. Mesh independence test was conducted to ensure reliability. The disinfection efficiency and aerosol concentration approximately remained the same if total element number was refined to 7.4 million and 10.2 million.

For two-stage ESP/HEFS system, the COMSOL platform was adopted to simulate corona discharge (ionized electric field), and ANSYS-FLUENT platform was utilized to simulate turbulent air flow and biological particle removal. Fig. 7 shows the mesh distributions of HEFS system. The hexahedral meshes were used. Local meshing refinement

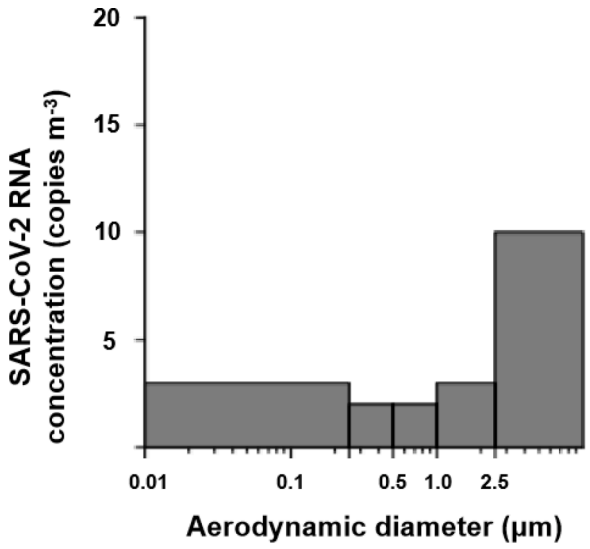

Fig. 8. Concentration of airborne SARS-CoV-2 RNA in different aerosol size bins (Liu et al., 2020).

was adopted around discharge wires and in the pleated filter medium zone. For simplicity, mesh distribution of two-stage ESP was not shown in this paper. The ionization ozone of two-stage ESP was the same to that of HEFS, and the same meshing strategy can be applied. For collection zone of ESP, the structural meshes were applied due to its regular geometry.

The boundary conditions for airflow modeling were straightforward: grounded plates, surfaces of discharge wire/UV lamp acted as stationary walls. The "Velocity Inlet" and "Pressure Outlet" types in ANSYS-FLUENT was respectively adopted for inlet and outlet of various system. For biological particle concentration, the dimensional inlet particle concentration ($1 \times 10^{\circ 4}$ (#/m^3)) was defined in each case, and "Outflow" type was applied for outlet. The problem of the corona discharge modeling was governed by two partial differential equations with unknown electric potential and space charge density. The boundary conditions for the electric potential were straightforward: a given applied voltage (V_P) on the discharge wires, zero potential on the grounded plates, zero-gradient boundary for surfaces of pleated filter. The Kaptzov hypothesis was used to calculate the boundary value of space charge density over the discharge wires-. This study used standard k-ε model to simulate air turbulence characteristics, and the SIMPLE algorithm to couple the pressure and velocity. The PRESTO! scheme was adopted for pressure discretization and the first-order upwind scheme for all the other variables. The enhanced wall functions were adopted with standard k-ε model since the y+ value was less than 30.

3. Results

3.1. Characteristics of SARS-CoV-2 aerosols

The characteristics of SARS-CoV-2 aerosols are necessary for numerical simulation of air cleaning devices. This includes aerodynamic characteristics and susceptibility to UV lights. Fig. 8 shows SARS-CoV-2 RNA concentration and aerodynamic size which were measured in Fangcang Hospital (Liu et al., 2020). The results indicate that SARS-CoV-2 aerosols were mainly found to include two size ranges, one in the sub-micron region (d_p between 0.25 and 1.0 μm) and the other in super-micron region ($d_p > 2.5$ μm). Based on sizes of SARS-CoV-2 aerosols and nature of RNA, the targeted aerosol size range in the current study was 0.1 μm to 2.5 μm. For airborne SARS-CoV-2 aerosols, there was no available experimental data on its susceptibility to UV lights. However, the effects of UV lights on the inactivation of

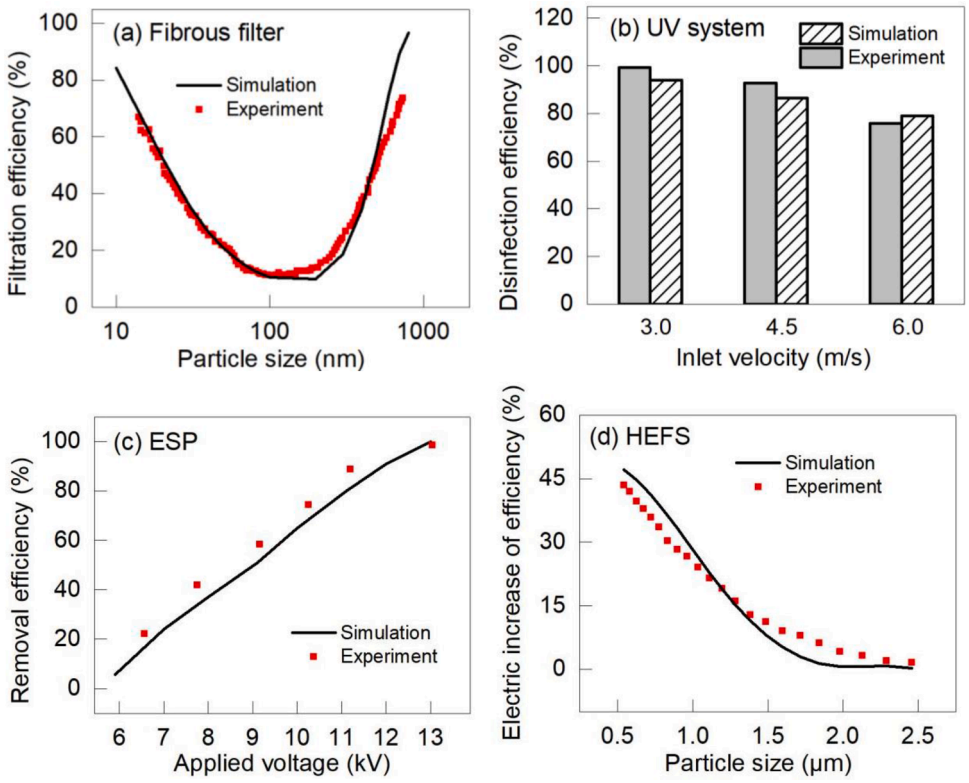

Fig. 9. Numerical validation of air cleaning devices: (a) Fibrous filter; (b) UV; (c) ESP; (d) HEFS.

SARS-CoV-2 aerosols deposited on solid surfaces and porous mediums were investigated experimentally (Fischer et al., 2020). The related experimental data was used in simulation of UV+HEPA system which was described in the following section.

3.2. Validation of numerical models for different air purification systems

Extensive numerical simulations were performed in order to study the filtration efficiency of the four filters, including: flat fibrous filter (HEPA), ESP, HEFS and UV. Fig. 9 compares the experimental and simulated filtration efficiency/disinfection efficiency of four air cleaning devices. The experimental data were based on previous researches (Feng et al., 2018b; Long & Yao, 2010; Yang et al., 2018).

Fig. 9(a) shows that there is agreement in terms of the filtration efficiencies predicted by numerical models and the experimental data. Filtration efficiency of a clean, flat filter was investigated, without considering the particle clogging process. The discrepancies between numerically simulated and experimentally measured data shown in Fig. 9(a) resulted from model errors induced by single-fiber efficiency formulas, as reported by Park, Yoon, and Hwang, (2011). Fig. 9(b) shows that the numerical model could reasonably predict disinfection efficiency of UV system (Yang et al., 2018). *Staphylococcus epidermidis* (ATCC 12228) was the selected bacteria type, with susceptibility of 0.37 (m^2/J). The disinfection efficiency decreased with increase of inlet air velocity due to different residence time. Fig. 9(c) compares simulated and measured particle removal efficiency of one-stage ESP (Long & Yao, 2010). Only one discharge wire was installed in ESP channel, and applied voltage varied from 6 kV to 13 kV. The seeded particle had a size of 4 μm. The discrepancies between simulated and experimental efficiency data were caused by errors of particle charging model (Long & Yao, 2010), which can be used to estimate electric charges carried by particles in ionized electric field. In Fig. 9(d), the "electric increase of efficiency" means filtration efficiency difference of fibrous filter in HEFS with/without applied voltage (Feng et al., 2016). In the numerical simulation of fibrous filter medium in HEFS, only the electrostatic effect of the target single fiber on charged particle motion was considered and the interaction with other charged fibers are ignored. The comparisons in Fig. 9 indicate that all numerical models could reasonably predict filtration/disinfection efficiency of each air cleaning device type. The validated simulation models were then used for the optimization and design of various air cleaning systems for indoor applications.

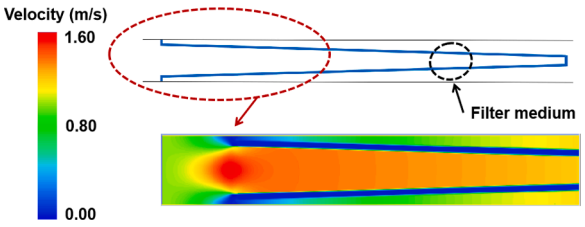

Fig. 10. Simulated air velocity distributions in one pleat of pleated fibrous filter (Filter-A).

3.3. Removal/disinfection performance of UV+Filter system

In UV+Filter system, airborne biological aerosols were treated (remove/disinfect) by three processes: 1) physical capture by fibrous filter due to filtration mechanism, 2) UV disinfection before reaching fibrous filter, and 3) UV dose applied to aerosols deposited in filter medium. These three processes could be analyzed individually because of different physical fields.

3.3.1. Physical capture by fibrous filter due to filtration mechanism

Firstly, physical filtration performance of UV+Filter system was described. Fig. 10 shows the simulated distributions of air velocity in one pleat channel of pleated fibrous filter. The maximum velocity magnitude (1.6 m/s) was observed in the entrance zone, which was higher than the inlet velocity (1.0 m/s). In filter medium, air velocity

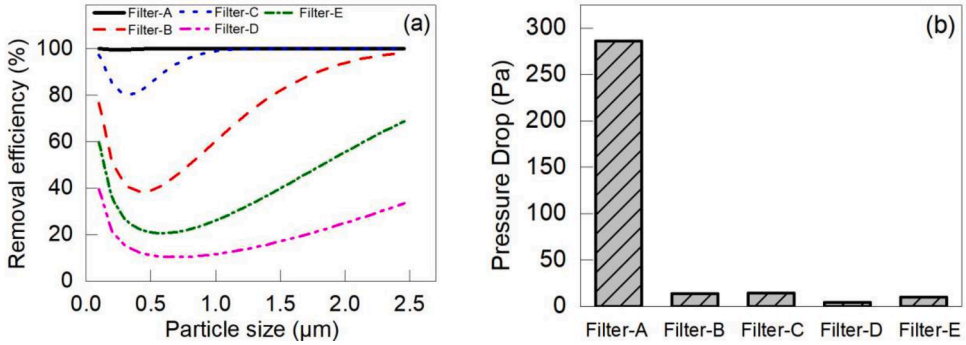

Fig. 11. Filtration performance of different air fibrous filter types: (a) filtration efficiency; (b) pressure drop. Filter A belongs to HEPA type, Filter B-C and D-E respectively belong to medium and coarse types.

(so-called filtration velocity) values become much lower due to large area of pleated filter medium. For filters with relatively high viscous resistance, filtration velocities were uniformly distributed along the surface of filter medium. For fibrous filters with a lower flow resistance, filtration velocities varied along the filter surface. Airflow field is the base of particle motion and filtration in filter.

Fig. 11 shows the simulated filtration performance of the five pleated fibrous filter: HEPA (Filter A), medium filter (Filter B, Filter C) and coarse filter (Filter D, Filter E). Size-dependent filtration efficiency and pressure drop were analyzed and compared. From Fig. 11(a), it can be observed that filtration efficiency was higher for very small (<0.3 μm) or large (>1.0 μm) particles. This trend was caused by the phenomena of particle diffusion and interception/impaction effects. Particle diffusion efficiency decreases with particle size while interception/impaction efficiency increases with particle size. For HEPA (Filter A), filtration efficiency was close to 100% for the whole particle size range. The MPPS (most penetrating particulate size) of Filter A was 0.3 μm and its filtration efficiency was 99.58%. For medium filter types, Filter C had a relatively high efficiency. The MPPS value of Filter C and the corresponding efficiency were 0.3 μm and 79.7%, respectively. The quality factor of Filter C was 0.38 which was much higher than that of Filter A (0.006). Quality factor is an index simultaneously integrating filtration efficiency and energy consumption (Feng et al., 2018b), as shown by Eq. (9). The overall performance of Filter C is better than Filter A (see Fig. 11 (a)). However, Filter C could not be recommended for the removal of SARS-CoV-2 aerosols due to its relatively low efficiency in the particle range of 0.2–0.6 μm (see Fig. 11(a)). SARS-CoV-2 aerosols were mainly found in two size ranges: 1) in submicrometre region (particle size between 0.25 and 1.0 μm) and 2) in supermicrometre region (particle size > 2.5 μm) (Liu et al., 2020). Therefore, it is necessary to utilize size-dependent efficiency curve to design fibrous filters in the SARS-CoV-2 control. Overall, pleated fibrous filter is a safe measure to use in ventilation systems for its high efficient removal of SARS-CoV-2 aerosols.

$$QF = -Ln(1 - eff)/(\Delta P Q_0) \tag{9}$$

where ΔP is the pressure drop across the fibrous filter medium (Pa), Q_0 is the unit air flow volume rate (1 m^3/s), the *eff* is the filtration efficiency for 0.3 μm particles.

Fig. 11(b) compares the pressure drops of the five fibrous filter types. Pressure drop and energy consumption are positively correlated. Commonly, filter types with a higher efficiency also have higher pressure drop. Filter A has a higher filtration efficiency while its pressure drop is much higher than those of other filter types. Utilization of Filter A (e.g. HEPA) in large quantities may cause considerate energy consumption therefore making it very necessary to develop high efficiency and energy-saving air cleaning devices towards the control of SARS-CoV-2 aerosols.

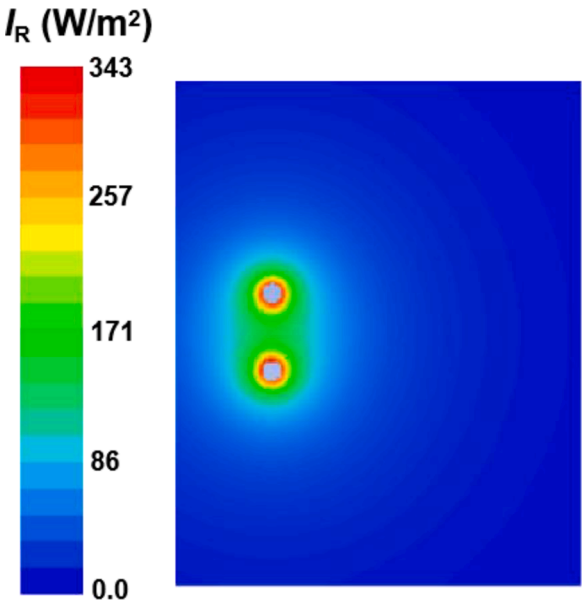

Fig. 12. Simulated distribution of UV irradiance intensity in UV+Filter system.

3.3.2. *UV disinfection before reaching fibrous filter*

Different from UV and ionized electric field, fibrous filter removes SARS-CoV-2 aerosols by physical filtration mechanisms (diffusion, interception and impaction) without biological disinfection effect. Survival and growth of SARS-CoV-2 in filter medium still remain unclear; some risks exist in the processes of air filter maintenance and replacement (Fischer et al., 2020). In the event of leakage in the filter medium, SARS-CoV-2 aerosols may penetrate filters and can cause serve danger to building occupants. It is therefore necessary to consider the risks of pleated fibrous filter in the operation process.

Fig. 12 shows the simulated distributions of irradiance intensity (I_R) in UV+Filter systems. Numerical results indicated that irradiance intensity decreased from lamps to duct surface. For UV disinfection simulation, the most challenging issue is to determine susceptibility "*A*", as shown in Eq. (5). Previous research utilized experimental methods to obtain the "*A*" value of five airborne biological bacteria types (*Serratia marcescens, Pseudomonas alcaligenes, Escherichia coli, Salmonella enterica*, and *Staphylococcus epidermidis*), which were exposed to UV light (Yang et al., 2018). The available literature has not yet reported disinfection experiments of ultraviolet germicidal irradiation on airborne SARS-CoV-2 aerosols in ventilation systems. Therefore, it is quite difficult to directly obtain accurate "*A*" value from available experimental research, which focused on UV inactivation of airborne SARS-CoV-2.

Previous studies made some assumptions regarding an appropriate value of the "*A*" value in order to investigate the effects of upper-room

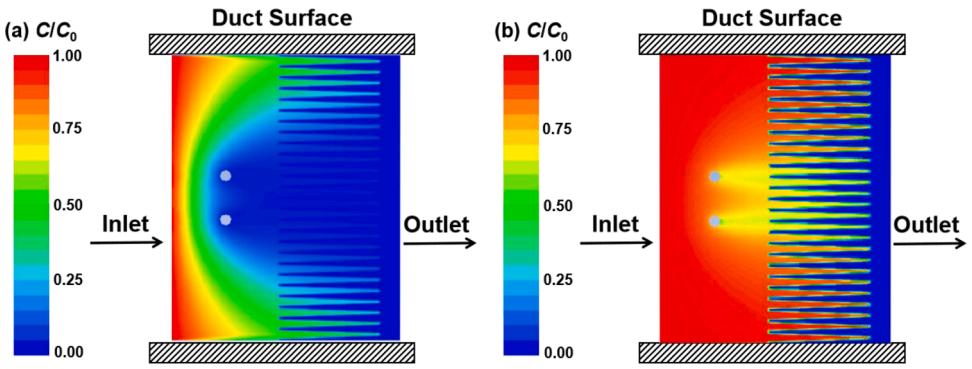

Fig. 13. Simulated concentration distribution of airborne SARS-CoV-2 aerosols in in-duct UV+Filter devices, (a) susceptibility "*A*" was 0.59 (m^2/J), (b) susceptibility "*A*" was 0.0377 (m^2/J).

ultraviolet air disinfection system on the reduction of COVID-19 transmission (Beggs & Avital, 2020). Based on the published literature regarding UV inactivation of different aerosolised corona-viruses, the range of "*A*" value was 0.377–0.590 (m^2/J). If "safety factor" was considered in the analysis, the range of "*A*" value was expanded to 0.0377–0.590 (m^2/J) (Beggs & Avital, 2020). This range of "*A*" value (0.0377–0.590 (m^2/J)) was adopted in simulation of COVID-19 disinfection by using upper-room ultraviolet air disinfection system (Beggs & Avital, 2020). Based on previous study, the current study simulated disinfection efficiency of an in-duct UV+Filter system with two "*A*" values: 0.0377 and 0.590 (m^2/J). Fig. 13 shows the numerically simulated dimensionless concentration distributions of airborne SARS-CoV-2 aerosols in-duct UV+Filter devices with different susceptibility values. *C* and C_0 were SARS-CoV-2 aerosols concentration of interior space and inlet, respectively. When "*A*" was 0.59, 81% of incoming SARS-CoV-2 aerosols were disinfected before reaching the pleated filter, and this efficiency decreased to 15% with "*A*" of 0.0377. The upper-room UVGI disinfection efficiency reported by previous research was higher than those of the in-duct UV device in this study, as shown in Fig. 13 (Beggs & Avital, 2020). The reason was that particle residence time (several minutes) of upper-room UVGI system was much higher than that (lower than one second) of in-duct UV devices. Due to the uncertainty of "*A*" value of airborne SARS-CoV-2 aerosols, it is difficult to reliably design in-duct UV system towards control of SARS-CoV-2. Therefore, it is necessary to investigate the accurate "*A*" value of airborne SARS-CoV-2 aerosols.

3.3.3. *UV dose applied to aerosols deposited in filter medium*

For airborne bacteria/virus, if the applied UV irradiation dose is enough, aerosols/particles are effectively inactivated. UV irradiation dose is the product of UV irradiation flux (W/m^2) and exposure time (s) (Beggs & Avital, 2020). Similarly, bacteria/virus deposited on solid surfaces or within fibrous filters is inactivated if UV irradiation dose is enough. In practical design, UV irradiation dose is an essential factor which can be used to determine whether the virus is dead or alive. However, the quantitative experiments focusing on UV inactivation of airborne SARS-CoV-2 aerosols is not available in literature. Recently, some researchers conducted experimental studies on UV inactivation of SARS-CoV-2 aerosols deposited on solid surfaces and fibrous medium (e.g. filtering facepiece respirators). Fischer et al., 2020 found that UV light (260–285 nm) effectively inactivated SARS-CoV-2 virus in fabric filter medium with irradiance intensity of 5.5 W/m^2, and they reported that after 100 min, almost all the virus was inactivated in contaminated fabric medium.

While pleated fibrous filters are capable of removing aerosol particles including dust and microorganisms from indoor air environments, they can become reservoirs for potentially hazardous particles, including bacterial and fungal spores (Nakpan et al., 2019). Several studies have shown that stress-resistant spores can remain viable over a

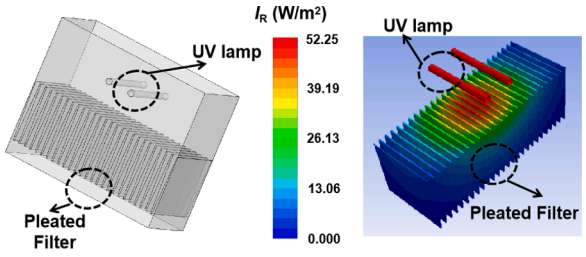

Fig. 14. Simulated distribution of UV irradiance intensity on pleat filter surface of UV+Filter system.

prolonged period of time and even grow in the filter media (Forthomme et al., 2014). The spores collected on filters can be re-aerosolized during replacement or maintenance (Morisseau, Joubert, Le Coq, & Andres, 2017), thereby posing a health risk. In order to overcome this disadvantage of pleated fibrous filter, UV+Filter system is developed for indoor ventilation systems. In a ventilation system, pleated filter loaded with virus/bacteria can be exposure to UV radiation for long time (e.g. several days/hour, operation time). For biological species deposited in filter medium, exposure time is long enough to deactivate virus/bacteria. Overall, UV generator in UV+Filter system could improve the safety level of fibrous filter due to biological inactivation effect.

Fig. 14 shows the simulated distributions of irradiance intensity (I_R) on pleated filter surface of UV+Filter system. The minimum I_R value on the pleated filter surface was 5.5 W/m^2, which was approximately the same as critical irradiance intensity value in previous literature (Fischer et al., 2020). In UV+HEPA system, SARS-CoV-2 aerosols were removed/destroyed by three mechanisms: 1) physical capture by fibrous filter due to filtration mechanism; 2) UV disinfection before reaching fibrous filter; and 3) UV dose applied to aerosols deposited in filter medium. Although the susceptibility "*A*" could be assumed by relevant experimental data, it is very necessary to obtain an accurate "*A*" value for engineering/operation safety. In the current design, only mechanisms (1–2) were considered. Mechanism (3) was not considered due to the lack of reliable susceptibility "*A*".

3.4. *Removal performance of electrostatic cleaning systems*

Fig. 15 shows the diagram of particle trajectory in two-stage ESP and simulated ion concentration distributions in ionization zone. Particles are charged in the ionization zone. In the collection zone, charged particles are driven by electric forces and move to collection plates. Due to relatively high inlet velocity (1 m/s), approximately none of incoming particles were deposited in the ionization zone. Although the well-designed one-stage ESP (e.g. including ionization zone only, as shown in Fig. 5) would have higher efficiency for particles in the submicrometre region, the large amount of generated ozone may harm

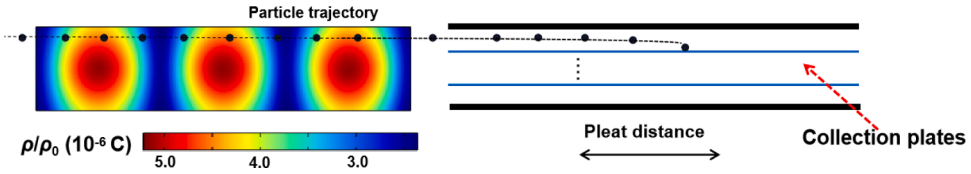

Fig. 15. The diagram of particle trajectory/removal in two-stage ESP and ion distributions in ionization zone.

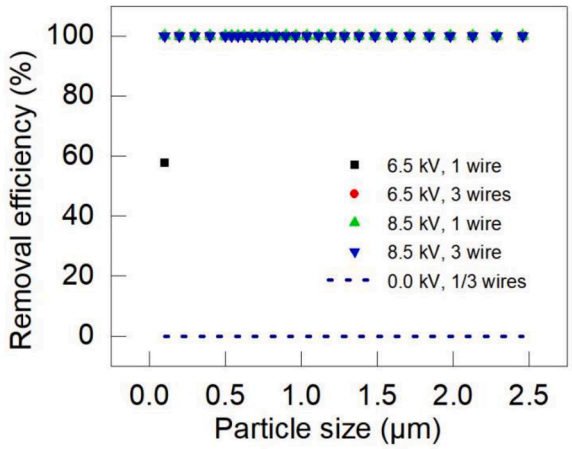

Fig. 16. Particle removal performance of two-stage ESP with collection length of 1 m.

human health.

Fig. 16 shows simulated particle removal performance of two-stage ESP with collection length of 1.0 m. The design parameters were: 6.5/8.5 kV (V_i), 1.0 m (collection length), and three discharge wires in the ionization stage. Except for ESP with single wire and applied voltage of 6.5 kV, all the values of size-dependent filtration efficiency were 100%, as shown in Fig. 16. The size-dependent efficiency of 0.1 μm particles was 57.7%, with applied voltage of 6.5 kV and one discharge wire. Considering the energy consumption and ozone generation, the optimal parameters for two-stage ESP were: applied voltage of 6.5 kV, and three discharge wires in ionization stage. Based on the previous study, the extra ozone generation (difference of ozone concentrations between ESP inlet/outlet) was lower than 8 ppb (Feng et al., 2016). Once the corona breakdown occurs (applied voltage decreases to zero), size-dependent particle removal efficiency decreases to 0, as shown by Fig. 16. Therefore, product quality of high-voltage generator/monitor must be guaranteed.

Fig. 17 describes simulated particle removal performance of HEFS. When the applied voltage was 0 kV, particle removal efficiency equaled to mechanical filtration efficiency. If three discharge wires were adopted, size-dependent filtration efficiency was close to 100%. Based on numerical results shown in Fig. 17, three design patterns of HEFS have filtration efficiency of 100%, including 8.5 kV/single wire, 8.5 kV/three wires, 6.5 kV/three wires. Energy consumption and ozone production of the HEFS design (6.5 kV/three wires) was found to be the least due to its low applied voltage. In regard to energy consumption and ozone generation, the HEFS with three discharge wires and applied voltage of 6.5 kV was selected as the optimal design.

Different from fibrous filter with mechanical filtration mechanism, HEFS or two-stage ESP have two air cleaning mechanisms: physical removal and biological disinfection. The biological disinfection mechanism on airborne microorganisms is associated with density of space charge or ions (Zhou et al., 2016). For numerical simulations of biological disinfection by ions, the most challenging issue is in determining the susceptibility values. Previous studies utilized experimental data to obtain susceptibility for a certain type of airborne biological aerosols (Zhou et al., 2016). However, the experimental data for airborne SARS-CoV-2 aerosols is lacking and previous research used assumed values to predict disinfection efficiency (Beggs & Avital, 2020). In order to ensure engineering safety, only physical removal mechanisms were considered in design of two-stage ESP and HEFS in this study.

4.Discussion

4.1. Comparison of various air cleaning devices

This study numerically investigated the overall performances of different air cleaning devices (Fibrous-filter, UV+Filter, two-stage ESP and HEFS) for removal of SARS-CoV-2 aerosols and compared them in term of filtration efficiency, energy consumption and secondary pollution. In comparison, designs of pleated fibrous filters in Fibrous-filter and UV+Filter systems were kept the same (Filter type A, high-efficient filter, pleat height of 100 mm, and pleat distance of 10 mm). For HEFS, the medium-efficient filter materials were used, which was described in detail in the methodology part. In numerical simulations of all air cleaning devices, inlet velocity was 1 m/s, and incoming air flow rate was 1 m^3/s. For two-stage ESP, critical design parameters were: applied voltage in ionization stage was 6.5 kV, collection length was 1 m, three wires was installed in ionization stage. For HEFS, critical design parameters were: applied voltage in ionization stage was 6.5 kV, three wires was installed in ionization stage.

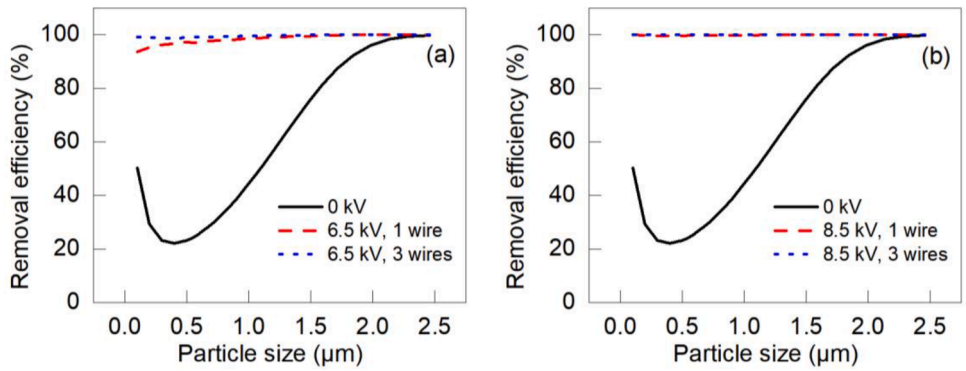

Fig. 17. Filtration performance of HEFS with different discharge wires: (a) 6.5 kV in ionization zone; (b) 8.5 kV in ionization zone.

Table 2
Comparison of different systems with optimal design from the perspectives of SARS-CoV-2 control.

System type	Particle removal efficiency (%, 0.1–2.5 μm)	Energy consumption (W)	Length of system (m)	Main Risks
Fibrous-filter	100	286.0	0.15	Re-Aerosolization
Two-stage ESP	100	6.1	1.30	Electric breakdown
HEFS	100	44.1	0.45	Electric breakdown
UV+Filter	100	483	0.30	N

For all the four systems with proper design parameters, the filtration/removal efficiency of 0.1–2.5 μm particles was approximately 100%. Table 2 compares the four proposed systems in terms of energy consumption, system space, and operation risk. The total required power (W) of air cleaning system includes the fan, high-voltage generator, and UV lamp. Detailed information about energy consumption calculation could be found in previous literature (Feng et al., 2018b; Yang et al., 2018).

Based on energy consumption, system ranking is UV+Filter > Fibrous-filter > HEFS > ESP. ESP and HEFS could save 97.8% and 84.6% of the energy consumed by Fibrous-filter. Due to UV irradiation, energy consumption of UV+Filter system was higher than Fibrous-filter. Two-stage ESP occupied much more space than the other system because of its length of collection plates. Although ESP was energy-efficient, its risk level was high. Once electric breakdown occurred, removal efficiency for all particle sizes decreased to zero. It is therefore necessary to adopt real-time monitoring of electric breakdown during the operation stage. The energy saving rate of HEFS was not as high as the two-stage ESP while its risk level was also lower. Once electric breakdown occurred, removal efficiency of HEFS was the same to that of medium-efficient filter, as shown in Fig. 17, and a large portion of incoming particles could be captured by the non-electrostatic fibrous filter. The risk of Fibrous-filter is re-aerosolization of deposited particles (e.g. spore) during replacement or maintenance (Morisseau, Joubert, Le Coq, & Andres, 2017). Professional property service and system maintenance were needed for Fibrous-filter users. UV+Filter system could significantly reduce risk, although its energy consumption was highest among the different air cleaning devices in Table 2. Based on risk level, system ranking is ESP > HEFS > Fibrous-filter > UV+Filter.

Due to the fact that ESP or HEFS releases some low-concentration ozone, they could not be used as portable air cleaning devices, which are directly placed in indoor environment. For large-scale public buildings with high energy consumption, two-stage ESP or HEFS are recommended in a central air conditioning system. ESP/HEFS could save a lot of energy and the relatively high level of property maintenance can ensure proper operation of filters. Fibrous-filter is recommended to be used in residential buildings, such as home-portable air purifiers. For replacement or maintenance of fibrous-filter, professional services are necessary to avoid secondary pollution. For extremely important occasions (e.g. hospital, biology laboratory and built environments during epidemics), UV+Filter system is recommended from the perspectives of safety and high-efficiency. In engineering applications, designers should simultaneously consider filtration/disinfection effect, energy consumption, installation space, risk level and practical need of users.

4.2. Limitations and prospects

In electrostatic removal systems (two-stage ESP and HEFS), airborne SARS-CoV-2 aerosols could be removed by electric force acting on charged particles. Once the biological aerosols are captured by electrostatic removal systems, these aerosols are considered to be filtered and not harmful for indoor environment. Actually, the ionized electric field could disinfect airborne biological aerosols and biological particles deposited in electrostatic removal systems. In the current study, only the aerosol removal performances of ESP/HEFS was considered. In future research, the biological disinfection effect (SARS-CoV-2 aerosols expose to ions and electric field) should be investigated.

Except for two-stage ESP and HEFS, many advanced types of electrostatic assisted air filtration systems have been developed (Mo, Tian, & Pan, 2020; Tian, Mo, & Li, 2018), including electrostatics assisted metal foam coarse filter, ESP with dielectric coatings et al. The experimental results indicated that these newly developed systems can reduce energy consumption without sacrificing particle removal efficiency. Besides, these advanced electrostatic assisted air filtration systems may be capable of high-efficiently disinfecting airborne species due to ion generation. Compared to the ESP/HEFS, these newly proposed electrostatic removal systems may have potential to be much more effective in control of airborne SARS-CoV-2 aerosols. Therefore, it is necessary to evaluate these systems from the perspectives of aerosol removal, disinfection efficiency and energy consumption. However, the numerical models utilized in the current study could not completely predict the complex multiple physical fields (e.g. foam filter) in these newly developed electrostatic filtration systems. In future, complete experiments will be conducted to evaluate removal/disinfection performance of various electrostatic assisted air filtration systems. Besides, numerical models will be improved to be capable of reasonably/accurately predicting the removal/disinfection efficiency of different electrostatic filtration systems.

Previous study (Luo & Zhong, 2021) concluded that air parameters (air temperature, relative humidity and air velocity) significantly influence the performance of UV system, including germicidal source output, UV rate constant, system inactivation efficiency, and system energy consumption. However, the effects of various air parameters were not considered in our current simulation study. In future, the numerical models will be improved to reasonably predict the performance of UV system under different air conditions.

In available literature, fibrous filters coated with photo-catalytic catalysts have been proven to be effective in air purification process (Zhong et al., 2018; Zhong, Haghighat, & Lee, 2013). Perhaps, the "UV+Filter" system with photo-catalytic catalysts coating may have much better performance from the perspectives of SARS-CoV-2 aerosol control. In our future study, we will investigate air purification performance of advanced fibrous filters (coated with photo-catalytic catalysts) towards the control of SARS-CoV-2 aerosols.

5. Conclusions

Considering the characteristics of SARS-CoV-2 aerosols (aerodynamic characteristics, susceptibility to UV lights), this study proposed a multiple-physics model to simulate overall performance of UV+Filter system, including aerosol filtration/disinfection efficiency and UV dose distribution on pleated filter medium. Besides, performances of different air cleaning systems (Fibrous-filter, ESP, HEFS, UV+Filter) were numerically simulated and compared. The following conclusions can be drawn as follows:

(1) For proper design (e.g. filter medium selection, pleat structure and UV configuration), filtration efficiency of UV+Filter was 100%, and UV dose applied to filter medium was sufficient to deactivate deposited SARS-CoV-2 aerosols.
(2) After proper design of each air cleaning type (e.g. filter medium selection, arrangement of discharge wires and applied voltage in ESP/HEFS), filtration/removal efficiency for particles sizing in [0.1 μm, 2.5 μm] could be as high as 100%. UV+Filter system could significantly reduce re-aerosolization risk of fibrous filter. The optimal systems were sorted based on potential risk: UV+Filter> Fibrous-filter>HEFS >ESP.

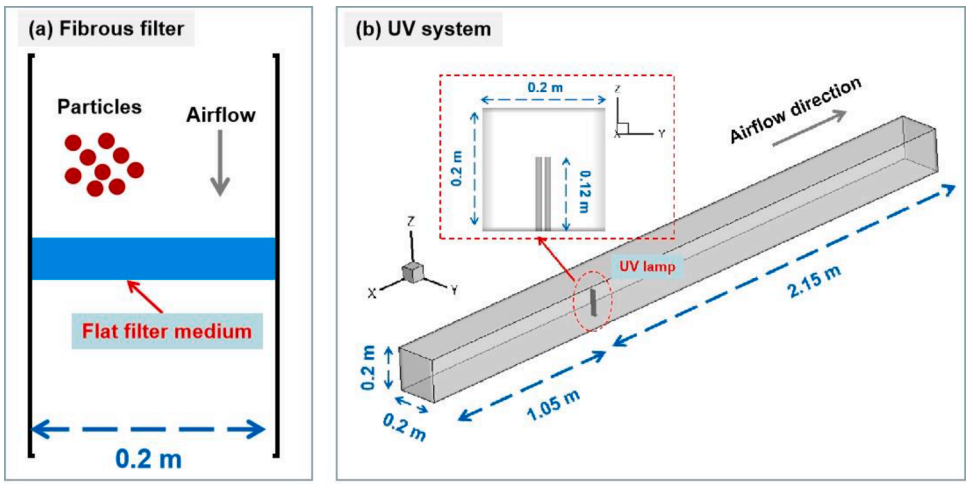

Fig. A1. The geometry of fibrous filter (Feng et al., 2018a) and UV system (Yang et al., 2018) in the numerical validation cases.

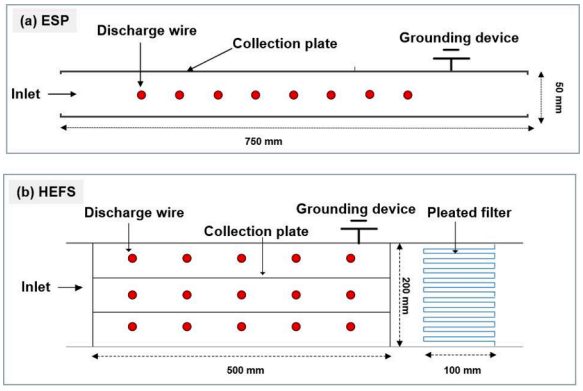

Fig. A2. The geometry of ESP (Long & Yao, 2010) and HEFS system (Feng et al., 2018b) in the numerical validation cases.

(3) The optimal systems were sorted based on energy consumption: UV+Filter> Fibrous-filter>HEFS>ESP. ESP and HEFS could save 97.8% and 84.6% of the energy consumed by Fibrous-filter. However, ESP/HEFS releases low-concentration ozone (below the critical value in standards) and induce risk of electric breakdown.

(4) Based on the simulated overall filtration/removal performance of different air cleaning types, their advantages/disadvantages and usage recommendations were summarized. The systematic selection, optimization and evaluation method of air cleaning systems proposed in the current study could provide essential tools and quantitative results for control of SARS-CoV-2 aerosols and other airborne disease types. For electrostatic removal systems, the biological disinfection effect (SARS-CoV-2 aerosols expose to ions and electric field) should be investigated in future research.

Declaration of Competing Interest

The author(s) declared no potential conflicts of interest with respect to the research, authorship, and/or publication of this article.

Acknowledgments

The authors would like to acknowledge the coordinated support from Natural Science Foundation of China (Grant No. 51808138; Grant No. 51778385), Basic and Applied Basic Research Fund of Guangdong Province (Grant No. 2019A1515011832).

Appendix

A1. Detailed information for cases of numerical validation

For fibrous air filter simulation, the numerical validation case was from previous literature (Feng et al., 2018a). The flat filter medium (glass-fiber material) was used, as shown in Fig. A1. The key parameters of filter medium were: (d_f: 3 μm; α: 0.035; Z: 500 μm). The standard k-ε model, together with Eq. (1) in this paper, were used to simulate turbulent airflow field in fibrous filter. The Lagrangian model (Eq. (2)) and particle filtration model (Eq. (3)) were simultaneously utilized to simulate particle motion and filtration in porous filter medium. The detailed information about how to integrating Lagrangian model and filtration model in ANSYS platform could be found in literature (Feng et al., 2018a). The inlet air velocity was fixed as 0.4 m/s, which was equal to the filtration air velocity of flat filter medium. The targeted particle sizes ranged from 10 nm to 1000 nm.

For UV device simulation, the numerical validation case was from previous literature Yang et al., 2018). The in-duct UV lamps were utilized to disinfect airborne biological aerosols. The UV generator consisted of twin tubes with 10 mm diameter and 120 mm luminous length. The irradiance intensity near lamp surface was close to 550 (W/m^2). The duct was made of galvanized steel with a 200 × 200 mm cross section. The detailed information about spatial position could be found in Fig. A1 or literature. *Staphylococcus epidermidis* (ATCC 12228) was the selected bacteria type, with susceptibility of 0.37 (m^2/J). The standard k-ε model was used to simulate turbulent airflow field, and Eqs. (4) and ((5) were respectively utilized to simulate UV irradiance distributions and aerosol motion/disinfection. Based on literature, three-dimensional geometry and meshing strategy was adopted. All tested bacteria were assumed to be spherical with a 1.0 μm diameter and 1000 kg/m^3 density (Yang et al., 2018). The inlet velocity magnitudes of ducts were 3.0, 4.5 and 6.0 m/s.

For HEFS simulation, the numerical validation case was from previous literature Feng et al., 2018b). The length of the ionization stage was 500 mm, and its cross section was 200 × 200 mm^2, as shown in Fig. A2(b). The ionization stage consisted of three channels, and there were five wires along

the center line in each channel. The discharge wires with 0.05 mm diameter were made of copper. The key parameters of filter medium were: (d_f: 10 μm; α: 0.14; Z: 2 mm; Pleat height: 100 mm; Pleat distance: 22.3 mm). The standard k-ε model was used to simulate turbulent airflow field, and Eqs. (6) and ((7) in this paper were respectively utilized to simulate electric potential and space charge concentration. The Lagrangian model (Eq. (2)), particle charging model (Eq. (8)) and particle filtration model (Eq. (3)) were simultaneously utilized to simulate particle motion, charging and filtration in porous filter medium. The detailed information about how to integrating Lagrangian model and electrostaic filtration model in ANSYS platform could be found in literature (Feng et al., 2018b). Fig. A2(a) shows the geometry of validation case of single-stage ESP (Long & Yao, 2010). Totally, eight corona discharge wires with 0.10 mm diameter were installed in the ESP channel. The simulation strategy of ESP was the same to that of the ionization stage of HEFS system.

A2. Detailed information for energy consumption calculation

The energy consumption of various air cleaning devices (UV+Filter, two-stage ESP, HEFS) were quantitatively evaluated in this section. In comparison, the same operation conditions were adopted: inlet velocity was 1 m/s, air flow rate was 1 m^3/s, and the targeted section area was 1 m^2. Many units of air cleaning devices should be added together to meet the requirements of targeted cross section with area of 1 m^2.

For the calculation of energy consumption of UV+Filter, the UV generator and fan (mechanical energy loss) was considered, as shown by Eq. (A1). The simulated results of pressure drop of filter and spatial irradiance of UV were utilized to calculate total energy consumption.

$$W = W_{UV} + W_{Fan} = I_R S k/\beta + PQ \tag{A1}$$

Where W (W) was the total energy consumption of UV+Filter, W_{UV} (W) and W_{Fan} (W) were respectively energy consumption of UV device and fan, I_R (W/m^2) and S were respectively irradiance intensity (UV lamp surface) and effective functional surface of UV lamp, P (Pa) and Q (m^3/s) were respectively pressure loss and airflow rate value of fibrous filter, k was the unit number needed to meet the requirement of cross section with area of 1 m^2 ($k = 4$ for the current study), β was UV conversion coefficient (β=0.433 recommended by manufacturer). In previous study (Yang et al., 2019), the β value was close to 0.42 based on calculation. For example (I_R=340 (V); $S = 0.0628$ (m^2); $k = 4$; β=0.433; $P = 286$ (Pa); $Q = 1$ (m^3/s)), the total energy consumption of UV+Filter was 483 (W).

For the calculation of energy consumption of HEFS, the high voltage generator and fan (mechanical energy loss) was considered, as shown by Eq. (A2). For two-stage ESP, only the electric energy consumed by high voltage generator was included in energy calculation. The simulated results of discharge current value, pressure drop of filter were utilized to calculate total energy consumption.

$$W = W_{HV} + W_{Fan} = VIk + PQ \tag{A2}$$

Where W (W) was the total energy consumption of HEFS, W_{HV} (W) and W_{Fan} (W) were respectively energy consumption of high voltage generator and fan, V (V) and I (A) were respectively applied voltage and current value of high voltage generator, P (Pa) and Q (m^3/s) were respectively pressure loss and airflow rate value of HEFS, k was the unit number needed to meet the requirement of cross section with area of 1 m^2 ($k = 15$ for the current study). For example ($V = 6500$ (V); $I = 0.0000627$ (A); $k = 15$; $P = 38$ (Pa); $Q = 1$ (m^3/s)), the total energy consumption of HEFS with three discharge wires was 44.1 (W). For pure fibrous filter and two-stage ESP, only the terms of PQ and VIK (Eq. (A2)) were respectively used in calculation of energy consumption.

References

Abdolghader, P., Haghighat, F., & Bahloul, A. (2018). Predicting fibrous filter's efficiency by two methods: Artificial neural network (ANN) and integration of genetic algorithm and artificial neural network (GAINN). *Aerosol Science and Engineering, 2*, 197–205.

ASHRAE. (2017). *American Society of Heating, Refrigerating and Air-conditioning Engineers (ASHRAE) STD 52.2: Method of testing general ventilation air-cleaning devices for removal efficiency by particle size*. Atlanta, GA: ASHRAE.

Bahrami, A., Haghighat, F., & Bahloul, A. (2021). Vacuum cleaner as a source of abiotic and biological air pollution in buildings - A review. *Advances in Building Energy Research*. https://doi.org/10.1080/175-12549.2020.1863859

Beggs, C., & Avital, E. (2020). Upper-room ultraviolet air disinfection might help to reduce COVID-19 transmission in buildings: A feasibility study. *PeerJ*. https://doi.org/10.7717/peerj.10196

Beria, P., & Lunkar, V. (2020). Presence and mobility of the population during the first wave of Covid-19 outbreak and lockdown in Italy. *Sustainable Cities and Society*, Article 102616. *accepted*.

Bhattacharyya, S., Dey, K., Paul, A. R., & Biswas, R. (2020). A novel CFD analysis to minimize the spread of COVID-19 virus in hospital isolation room. *Chaos, Solitons & Fractals, 139*, Article 110294.

Buonanno, G., Stabile, L., & Morawsk, L. (2020). Estimation of airborne viral emission: Quanta emission rate of SARS-CoV-2 for infection risk assessment. *Environment International, 141*, Article 105794.

Cao, S. J., & Ren, C. (2018). Ventilation control strategy using low-dimensional linear ventilation models and artificial neural network. *Building and Environment, 144*, 316–333.

CDC, (2019). Manufacturing workers and employers, Interim guidance from CDC and OSHA, accessed May/30/2020. https://www.cdc.gov/coronavirus/2019-ncov/community/guidance-manufacturing-workers-employers.html.

Charvet, A., Pacault, S., Bourrous, S., & Thomas, D. (2018). Association of fibrous filters for aerosol filtration in predominant Brownian diffusion conditions. *Separation and Purification Technology, 207*, 420–426.

Chen, L., Gonze, E., Ondarts, M., Outin, J., & Gonthier, Y. (2020). Electrostatic precipitator for fine and ultrafine particle removal from indoor air environments. *Separation and Purification Technology, 247*, Article 116964.

Correia, G., Rodrigues, L., Gameiro, M., & Gonçalves, T. (2020). Airborne route and bad use of ventilation systems as non-negligible factors in SARS-CoV-2 transmission. *Medical Hypotheses, 141*, Article 109781.

Ding, J., Yu, C. W., & Cao, S.-. J. (2020). HVAC systems for environmental control to minimize the COVID-19 infection. *Indoor and Built Environment, 29*, 1195–1201.

Feng, Z., Cao, S-J., Wang, J., Kumar, P., & Haghighat, F. (2021). Indoor airborne disinfection with electrostatic disinfector (ESD): Numerical simulations of ESD performance and reduction of computing time. *Building and Environment, 200*, Article 107956. https://doi.org/10.1016/j.buildenv.2021.107956

Feng, Z., Long, Z., & Yu, T. (2016). Filtration characteristics of fibrous filter following an electrostatic precipitator. *Journal of Electrostatics, 83*, 52–62.

Feng, Z., Pan, W., Wang, Y., & Long, Z. (2018a). Modeling filtration performance of pleated fibrous filters by Eulerian-Markov method. *Powder Technology, 340*, 502–510.

Feng, Z., Pan, W., Zhang, H., Cheng, X., Long, Z., & Mo, J. (2018b). Evaluation of the performance of an electrostatic enhanced air filter (EEAF) by a numerical method. *Powder Technology, 327*, 201–214.

Feng, Z., & Cao, S-J. (2019). A newly developed electrostatic enhanced pleated air filters towards the improvement of energy and filtration efficiency. *Sustainable Cities and Society, 49*, Article 101569. https://doi.org/10.1016/j.scs.2019.101569

Fischer, R., Morris, D., Doremalen, N., Sarchette, S., Matson, M., Bushmaker, T., et al. (2020). Effectiveness of N95 respirator decontamination and reuse against SARS-CoV-2 Virus. *Emerging Infectious Diseases, 29*, 2253–2255.

Forthomme, A., Joubert, A., Andrès, Y., Simon, X., Duquenne, P., Bemer, D., et al. (2014). Microbial aerosol filtration: Growth and release of a bacteria-fungi consortium collected by fibrous filters in different operating conditions. *Journal of Aerosol Science, 72*, 32–46.

GB/T 13554-2020, (2020). High efficiency particulate air filter, National standard of the People's Republic of China.

Heilingloh, C., Heilingloh, U., Schipper, L., Dittmer, U., Witzke, O., Yang, D., et al. (2020). Susceptibility of SARS-CoV-2 to UV irradiation. *American Journal of Infection Control, 48*, 273–1275.

Hosseini, M. R., Fouladi-Fard, R., & Aali, R. (2020). COVID-19 pandemic and sick building syndrome. *Indoor and Built Environment, 29*, 1181–1183.
Leng, J., Wang, Q., & Liu, K. (2020). Sustainable design of courtyard environment: From the perspectives of airborne diseases control and human health. *Sustainable Cities and Society, 62*, Article 102405.
Liu, Y., Ning, Z., Chen, Y., Guo, M., Liu, Y., & Gali, N. (2020). Aerodynamic analysis of SARS-CoV-2 in two Wuhan hospitals. *Nature, 582*, 557–560.
Loey, M., Manogaran, G., Taha, M. H. N., & Khalifa, N. E. M. (2020). Fighting against COVID-19: A novel deep learning model based on YOLO-v2 with ResNet-50 for medical face mask detection. *Sustainable Cities and Society*, Article 102616. *accepted*.
Long, Z., & Yao, Q. (2010). Evaluation of various particle charging models for simulating particle dynamics in electrostatic precipitators. *Journal of Aerosol Science, 41*, 702–718.
Luo, H., & Zhong, L. (2021). Ultraviolet germicidal irradiation (UVGI) for in-duct airborne bioaerosol disinfection: Review and analysis of design factors. *Building and Environment, 197*, Article 107852.
Luo, X., Huang, X., Feng, Z., Li, J., & Gu, Z. (2021). Influence of air inlet/outlet arrangement of displacement ventilation on local environment control for unearthed relics within site museum. *Energy and Buildings, 246*, Article 111116.
Malayeri, M., Haghighat, F., & Lee, C. (2021). Kinetic modeling of the photocatalytic degradation of methyl ethyl ketone in air for a continuous-flow reactor. *Chemical Engineering Journal, 404*, Article 126602.
Malayeri, M., Lee, C. S., Haghighat, F., & Klimes, L. (2020). Modeling of gas-phase heterogeneous photocatalytic oxidation reactor in the presence of mass transfer limitation and axial dispersion. *Chemical Engineering Journal, 386*, Article 124013.
Mo, J., Tian, E., & Pan, J. (2020). New electrostatic precipitator with dielectric coatings to efficiently and safely remove sub-micro particles in the building environment. *Sustainable Cities and Society, 55*, Article 102063.
Morisseau, K., Joubert, A., Le Coq, L., & Andres, Y. (2017). Quantification of the fungal fraction released from various preloaded fibrous filters during a simulated ventilation restart. *Indoor Air, 27*, 529–538.
Nakpan, W., Yermakov, M., Indugula, R., Reponen, T., & Grinshpun, S. (2019). Inactivation of bacterial and fungal spores by UV irradiation and gaseous iodine treatment applied to air handling filters. *Science of the Total Environment, 671*, 59–65.
NCCEH, (2020). Physical barriers for covid-19 infection prevention and control in commercial settings, nat-ional collaborating centre for environmental health (NCCEH), accessed May/13/2020, https://ncceh.ca/-content/blog/physical-barriers-covid-19-infection-prevention-and-control-commercial-settings.
Park, J., Yoon, K., & Hwang, J. (2011). Removal of submicron particles using a carbon fiber ionizer-assisted medium air filter in a heating, ventilation, and air-conditioning (HVAC) system. *Building and Environment, 46*, 1699–1708.
Rahman, M. A., Zaman, N., Asyhari, A. T., Al-Turjman, F., Bhuiyan, M. Z. A., & Zolkipli, M. F. (2020). Data-driven dynamic clustering framework for mitigating the adverse economic impact of Covid-19 lockdown practices. *Sustainable Cities and Society, 62*, Article 102372.
Saleh, A., & Tafreshi, H. (2014). A simple semi-numerical model for designing pleated air filters under dust loading. *Separation and Purification Technology, 137*, 94–108.
Sarkis-Onofre, R., Borges, R., Demarco, G., Dotto, L., Schwendicke, F., & Demarco, F. (2020). Decontamination of N95 respirators against SARS-CoV-2: A scoping review. *Journal of Dentistry*. https://doi.org/10.1016/j.jdent.2020.103534
Shyegan, Z., Haghighat, F., & Lee, S. O. (2020). Carbon-Doped TiO_2 film to enhance visible and UV light photocatalytic degradation of indoor environment volatile organic compounds. *Journal of Environmental Chemical Engineering, 8*, Article 104162.
Tian, E., Mo, J., & Li, X. (2018). Electrostatically assisted metal foam coarse filter with small pressure drop for efficient removal of fine particles: Effect of filter medium. *Building and Environment, 44*, 419–426.
Velali, E., Dippel, J., Stute, B., Handt, S., Loewe, T., & Lieres, E. (2020). Model-based performance analysis of pleated filters with non-woven layers. *Separation and Purification Technology, 250*, Article 117006.
Vuorinen, V., Aarnio, M., Alava, M., Alopaeus, V., Atanasova, N., Auvinen, M., et al. (2020). Modelling aerosol transport and virus exposure with numerical simulations in relation to SARS-CoV-2 transmission by inhalation indoors. *Safety Science, 130*, Article 104866.
Wang, B., Haghighat, F., & Mortazavi, R. (2009). Evaluation of modeling and measurement techniques of ultraviolet germicidal irradiation effectiveness-towards the design of immune buildings. *Indoor and Built Environment, 18*, 101–112.
Wang, J. (2021). Vision of China' s future urban construction reform: In the perspective of comprehensive prevention and control for multi disasters. *Sustainable Cities and Society, 64*, Article 102511.
WHO. (2020). WHO considers 'airborne precautions' for medical staff after study shows corona virus can survive in air. https://www.cnbc.com/2020/03/16/who-considers-airborne-precautions-for-medical-staff-afte-r-study-shows-coronavirus-can-survive-in-air.html.
Wang, J., Huang, J., Feng, Z., Cao, S-J., & Haghighat, F. (2021). Occupant-density-detection based energy efficient ventilation system: Prevention of infection transmission. *Energy and Buildings, 240*, Article 110883. https://doi.org/10.1016/j.enbuild.2021.110883
Xu, C., Luo, X., Yu, C. W., & Cao, S.-. J. (2020). The 2019-nCoV epidemic control strategies and future challenges of building healthy smart cities. *Indoor and Built Environment, 29*, 639–644.
Yang, Y., Zhang, H., Chan, V., & Lai, A. (2019). Development and experimental validation of a mathematical model for the irradiance of in-duct ultraviolet germicidal lamps. *Building and Environment, 152*, 160–171.
Yang, Y., Zhang, H., Nunayon, S., Chan, V., & Lai, A. (2018). Disinfection efficacy of ultraviolet germicidal irradiation on airborne bacteria in ventilation ducts. *Indoor Air, 28*, 806–817.
Yeo, S., Hosein, L., & Gregor-Davies, L. (2020). Use of HEPA filters to reduce the risk of nosocomial spread of SARS-CoV-2 via operating theatre ventilation systems. *British Journal of Anaesthesia, 125*, 361–363.
Yüksel, A., Arıcı, M., Krajčík, M., & Karabay, H. (2020). Experimental investigation of thermal comfort and CO2 concentration in mosques: A case study in warm temperate climate of Yalova, Turkey. *Sustainable Cities and Society, 52*, Article 101809.
Zhao, B., Chen, C., Yang, X., & Lai, A. C. K. (2010). Comparison of three approaches to model particle penetration coefficient through a single straight crack in a building envelope. *Aerosol Science and Technology, 44*, 405–416.
Zhao, B., Liu, Y., & Chen, C. (2020). Air purifiers: A supplementary measure to remove airborne SARS-CoV-2. *Building and Environment, 177*, Article 106918.
Zhong, L., & Haghighat., F. (2018). Modeling of by-products from photocatalytic oxidation (PCO) indoor air purifiers: A case study of ethanol. *Building and Environment, 144*, 427–436.
Zhong, L., Haghighat., F., & Lee, C. S. (2013). Ultraviolet photocatalytic oxidation for indoor environment applications: Experimental validation of the model. *Building and Environment, 62*, 155–166.
Zhong, L., Lee, C. S., Haghighat, F., & Bahloul, A. (2016). Deactivation and ultraviolet C-induced regeneration of photocatalytic oxidation air filters. *Science and Technology for the Built Environment, 22*, 576–585.
Zhou, P., Yang, Y., Lai, A., & Huang, G. (2016). Inactivation of airborne bacteria by cold plasma in air duct flow. *Building and Environment, 106*, 20–130.